Published online June 29, 2007

Using the EM38DD Soil Sensor to Delineate Clay Lenses in a Sandy Forest Soil

L. Cockx*
M. Van Meirvenne
Dep. of Soil Management and Soil Care
Ghent Univ.
Coupure 653, 9000 Gent, Belgium

B. De Vos
Research Institute for Nature and Forest,
Gaverstraat 4
9500 Geraardsbergen, Belgium

The objective of this study was to locate clay lenses in a sandy forest soil. The study site was a Scots pine (*Pinus sylvestris* L.) plantation in the Campine region of Belgium, which has been selected as a European Union-funded Level II Research Site for soil monitoring. Typically, the soils in the area have homogeneous sandy soil profiles, but clay lenses occur locally within a depth of 2 m of the soil surface. Locating these clay lenses is necessary because they can have a substantial impact on soil processes. Therefore, we used the EM38DD soil sensor to measure the soil apparent electrical conductivity (ECa) simultaneously in two orientations. Apparent electrical conductivity maps were generated and it was found that the variation in ECa was mainly driven by the spatial variability of soil texture across the study site. The ratio of the two orientations (profile ratio or PR) clearly revealed a circular pattern with decreased PR values (<1), which was identified as a clay lens. To delineate the extent of this lens, two numerical methods were used: (i) a fuzzy-*k*-means classification of the PR map focusing on the lowest centroid class, and (ii) a probability approach through indicator kriging. Using a validation image obtained from directed auguring, cell-by-cell comparisons were made for these two methods complemented with spatial accuracy measures. Although both methods tended to underestimate the spatial extent of the clay lens, the indicator kriging method was the most accurate, with an overall accuracy of 0.838, a proportion of error due to locational errors (κ-loc) of 0.864, and an average similarity of 0.841.

Abbreviations: AUC, area under the curve; CEC, cation exchange capacity; ECa, apparent electrical conductivity; EC_h, electrical conductivity measurement in the horizontal orientation; EC_v, electrical conductivity measurement in the vertical orientation; EMI, electromagnetic induction; FPI, fuzziness performance index; GPR, ground penetrating radar; IK, indicator kriging;NCE, normalized classification entropy; OK, ordinary point kriging; PR, profile ratio; ROC, receiver operating characteristic; RNE, relative nugget effect.

PEDOLOGY

The spatial variability of forest soils is an important factor for forest site planning, quality, and productivity (Schoenholtz et al., 2000). Forest soils serve multiple production and environmental functions and maintaining these functions is crucial for sustainable forest management.

Accurate characterization of the soil is a preliminary step in site establishment, since both lateral and vertical soil heterogeneity may have an impact on tree growth patterns. Soil texture is a fundamental qualitative soil physical property, influencing many other properties and processes including soil formation, water movement, erosion potential, and cation exchange capacity (CEC). It strongly affects soil moisture and controls the pool of nutrients available for plant uptake (Mc Bride et al., 1990). Soil discontinuities may be defined by significant changes in soil texture, and their identification and spatial delineation is important in land use decision making (Ogg et al., 2000). The presence of a clay layer in a sandy soil constitutes a discontinuity that restricts infiltration and influences the lateral movement of soil water and agrochemicals (Doolittle et al., 1994). Concerning forest productivity, Woolery et al. (2002) selected clay content in the B horizon as an important parameter for estimating species productivity. Also, Bravo and Montero (2001) found texture to be an important factor for forest productivity. Generally, soil texture is known to determine the impact of soil disturbances on tree growth (Gomez et al., 2002). A potential consequence of soil compaction caused by harvesting or site preparation is the significant loss of site productivity. It should be mentioned, however, that forest productivity relies on the interplay of soil physical, chemical, and biological properties and processes, which can be complex and varying among forest ecosystems (Schoenholtz et al., 2000). Consequently, future forest management practices should be site specific and account for the spatial variability of soil properties. Therefore, knowledge of the spatial variability of soil texture may be important for interpreting tree productivity and planning forest management strategies.

New techniques have evolved that allow soil spatial variability to be identified using noninvasive, geophysical soil sensors. Sensors based on electromagnetic induction (EMI) have already proved their utility for soil characterization in agricultural soils (Corwin and Lesch, 2005). In this sensing technique, the bulk or apparent soil electrical conductivity (ECa)

Soil Sci. Soc. Am. J. 71:1314–1322
doi:10.2136/sssaj2006.0323
Received 12 Sept. 2006.
*Corresponding author (liesbet.cockx@ugent.be).

is measured, which is used as an indirect indicator of some soil properties (McNeill, 1980). In nonsaline soils, the variation in ECa is primarily determined by soil texture, moisture content, and CEC, all of which are important to plant biomass production. The inverse of ECa, the electrical resistivity, measured through direct current, can also be considered as a surrogate for the variability of soil physical properties (Samouëlian et al., 2005). Its depth of investigation depends on the distance between the electrodes, which is limited in densely populated forests by the inter-tree distance. On the other hand, ground-penetrating radar (GPR) has proved to be an effective tool for exploring subsurface horizons, also in forests (Butnor et al., 2003). Kung and Donohue (1991) showed that GPR was able to locate soil layers with textural discontinuities, whereas Boll et al. (1996) predicted the depth to textural interfaces using GPR. Both techniques detect changes in electromagnetic soil properties. The use of GPR is limited, however, since only electrically resistive soils are amenable to study (Butnor et al., 2003). As a response to this disadvantage, EMI has been used as a precursory tool to guide the more costly, complex, and time-consuming GPR measurements (Gish et al., 2002; Inman et al., 2002). Generally, it is recognized that EMI allows the detection of gradual lateral changes in textural properties (Doolittle and Collins, 1998), whereas GPR is better suited to vertical exploration of textural discontinuities. Nevertheless, several researchers (Brus et al., 1992; Bork et al., 1998; Mueller et al., 2003) have reported the use of EMI to find textural discontinuities within the soil profile.

This study performed both lateral and vertical soil explorations using an EMI sensor. The sandy soil of the study area is characterized by the presence of a clay lens at variable depth. We aimed to locate this textural discontinuity with the EM38DD sensor (Geonics Ltd., Mississauga, ON, Canada). This sensor has the advantage of measuring the ECa simultaneously in two orientations. The ratio of these two orientations provides an indirect measure of the degree of soil profile heterogeneity. Additionally, we investigated different data analysis techniques to delineate the spatial extent of the clay lens.

MATERIALS AND METHODS

Study Site

The study site is an even-aged, 75-yr-old Scots pine plantation of 2 ha in Brasschaat, Belgium (central coordinates: 51°18′33″ N, 4°32′14″ E). The plantation is part of a 150-ha mixed coniferous–deciduous state forest, called "De Inslag." Since 1988, the Flemish Research Institute for Nature and Forest has used this site as a research area and in 1992 it was integrated as a Level II Research Site into a European research program for monitoring forest ecosystems. Several studies concerning tree physiology, nutrient behavior, CO_2 and water cycles, forest vitality, and air pollution monitoring were conducted or are ongoing at this site.

The topography of the area is flat with a maximum height variation of 33 cm. The soil is a moderately wet sandy soil, characterized by an anthropologically disturbed spodic horizon, called a "post-podzol" in the Belgian soil classification (symbolized as Zegb on the Belgian soil map) or an Anthreptic Haplorthod according to the USDA Soil Taxonomy (Soil Survey Staff, 2003). The soil parent material is a homogeneous aeolian coarse sand, but at variable depths (usually from 1.5 to 2 m) clay with a thickness of at least 0.20 m can be found (>40% clay, with clay defined as particles with a diameter <2 μm). The origin of the sedimented clay is unclear. It is hypothesized to be the remains of a bed of small fens covered by sand in the Pleistocene epoch. The mineral soil is characterized by very low pH values (pH in H_2O between 3.6 and 4.1) and a very low CEC; the forest floor is of the Mor type and varies in thickness across the site (1–13 cm). At some locations, a thick moss layer (3–7 cm) covering the litter layer is present. In the northwestern corner, traces of Second World War activities were found.

Apparent Electrical Conductivity Survey

We conducted a soil sensing survey using the EM38DD electromagnetic induction sensor. The EM38DD sensor consists of two EM38 units fixed perpendicular to each other. In each unit a transmitter coil is energized with an alternating current, inducing a primary electromagnetic field. This induces very small currents in the soil, which generate a secondary electromagnetic field that is sensed by a receiver coil located 1 m from the transmitter coil. The ratio of the secondary to the primary fields provides a measure of the ECa of the soil.

With the EM38DD, the soil ECa is measured simultaneously in two orientations, each having its own depth response profile. The sensitivity of the sensor can reach a depth of 2 m in low-conductive soils. The vertical orientation (EC_v) receives its major influence from deeper soil layers, while the horizontal orientation (EC_h) receives a dominant influence of the near surface soil. Combining the ECa measured in the two orientations in a so-called profile ratio (PR) provides an indication of the heterogeneity of the soil profile (Corwin et al., 2003): PR = EC_h/EC_v. A PR close to 1 indicates a uniform profile, a PR < 1 indicates a more conductive subsoil compared with the topsoil and a PR > 1 indicates decreasing conductivity with depth.

In total, 156 ECa measurements were taken by putting the EM38DD manually on the soil surface. Fifty-four locations were selected on the basis of a predefined grid with a 20- by 20-m spacing; the other locations were taken between these grid nodes to complement the regular sampling design with shorter distance measurements.

Soil Sampling

To provide an interpretation of the ECa measurements, soil samples at 23 locations were taken at 50-cm intervals down to 2 m. Texture was analyzed using the conventional pipette method. Additionally, in the area where we expected to find a clay lens, the presence of heavy clay within a depth of 2 m was checked by hand auguring at 60 locations. Where a clay lens was encountered, the depth to its top was registered. These observations were used as validation data.

Interpolation Techniques

The ECa measurements were interpolated using ordinary point kriging (OK). This is a geostatistical method that provides an estimate of a variable Z at any unsampled location $\mathbf{x}_0$ using a linear combination of observations within a predefined neighborhood around $\mathbf{x}_0$ (Goovaerts, 1997). The spatial structure of Z is represented by a variogram model, which is used to assign a weight λ_α to the $n(\mathbf{x}_0)$ neighbors $Z(\mathbf{x}_\alpha)$, yielding the OK estimator:

$$Z^*_{\mathrm{OK}}(\mathbf{x}_0) = \sum_{\alpha=1}^{n(\mathbf{x}_0)} \lambda_\alpha Z(\mathbf{x}_\alpha) \qquad [1]$$

The sum of these weights must equal unity to guarantee that the predictor is unbiased.

Indicator kriging (IK) was used to obtain a map of the probability of occurrence of the clay lens in terms of a critical PR and to interpolate the categorical (binary) presence/absence data to a validation map showing the presence of heavy clay within 2-m depth. To obtain a probability map of PR, alternative methods like stochastic simulations or disjunctive kriging could be used as well; however, we used IK because it is conceptually quite simple and its performance was evaluated to be similar (Lark and Ferguson, 2004). The principles of IK have been discussed in detail by Goovaerts (1997), Deutsch and Journel (1998), and others. Indicator kriging obtains the probability of a certain critical threshold z_c being exceeded by building the conditional cumulative distribution function (ccdf) at each point based on the behavior and correlation structure of indicator-transformed data. The ccdf $F[\mathbf{x}_0; z|(n)]$ signifies a probabilistic model for the uncertainty around the unknown value at $\mathbf{x}_0$, where $|(n)$ represents the conditioning to local information:

$$F\left[\mathbf{x}_0; z|(n)\right] = \text{Prob}\left[Z\left(\mathbf{x}_0\right) \le z|(n)\right] \quad [2]$$

Therefore, original data have to be transformed into indicators $i(\mathbf{x}_\alpha; z_k)$ in respect to a series of k threshold values z_k, selected across the range of data:

$$i(\mathbf{x}_\alpha; z_k) = \begin{cases} 1 & \text{if } z(\mathbf{x}_\alpha) \le z_k \\ 0 & \text{otherwise} \end{cases} \quad k = 1, 2, \ldots, K \quad [3]$$

Generally, the quantiles of the ccdf are taken as a series of k threshold values, covering the range of variation of z (Van Meirvenne and Goovaerts, 2001). For each threshold, an indicator variogram is modeled and ordinary IK estimates of the indicators are used to approximate the ccdf at the every point $\mathbf{x}_0$. After the ccdf is built, it must be post-processed to assess the probability that the estimation is larger, or smaller, than the critical threshold z_c.

Classification and Delineation Methods

Two numerical methods were used for the delineation of the clay lens from ECa measurements: (i) a fuzzy-*k*-means classification and (ii) a classification based on the probability of exceeding a critical threshold.

The fuzzy-*k*-means classification is an unsupervised classification used to identify "natural clusters" in a data set $\mathbf{X}$ (with elements x_{ig}; with $i = 1, \ldots, n$; $g = 1, \ldots, p$) having n individuals with p attributes (Bezdek, 1981). Each individual is allocated a membership [0,1] to each of the k clusters through an iterative algorithm starting with a random set of cluster means. Each individual is then assigned to the closest of these means and new means are recalculated based on the distance in attribute space between the individual and the cluster mean. This is repeated until a specified convergence criterion is met. The aim is to identify cluster centroids that minimize the generalized objective function, which is defined as follows:

Table 1. Two by two confusion matrix.

Predicted	Observed		Total
	Presence	Absence	
Presence	a = true positives	b = false positives	$a + b$
Absence	c = false negatives	d = true negatives	$c + d$
Total	$a + c$	$b + d$	$N = a + b + c + d$

$$J(\mathbf{M}, \mathbf{C}) = \sum_{i=1}^{n}\sum_{j=1}^{k} m_{ij}^{\varphi} d^2\left(x_i, c_j\right) \quad [4]$$

where $\mathbf{M}$ is the matrix with membership values m_{ij} (with $i = 1, \ldots, n$; $j = 1, \ldots, k$), $\mathbf{C}$ is the matrix of class centers c_{jg} (with $j = 1, \ldots, k$; $g = 1, \ldots, p$), $d^2(x_i, c_j)$ is the squared distance between each data point x_i and its cluster centroid c_j, and φ is the fuzzy exponent defining the degree of fuzziness of the solution. When $\varphi = 1$ the solution is a hard partition; as φ approaches infinity, the solution approaches its maximum degree of fuzziness. In this study, the Euclidean distance was taken as the distance measure because only one input variable ($p = 1$) was used. The optimum number of clusters is determined by minimizing two indices: the fuzziness performance index (FPI), which measures the degree of fuzziness, and the normalized classification entropy (NCE), which indicates the degree of fuzzification. The FPI is defined as follows (Roubens, 1982):

$$\text{FPI} = 1 - \frac{kF - 1}{k - 1} \quad [5]$$

where F is the partition coefficient:

$$F = \frac{1}{n}\sum_{i=1}^{n}\sum_{j=1}^{k} m_{ij}^2 \quad [6]$$

The NCE is defined as:

$$\text{NCE} = \frac{H}{\log k} \quad [7]$$

where H is the entropy function:

$$H = -\frac{1}{n}\sum_{i=1}^{n}\sum_{j=1}^{k} m_{ij} \log\left(m_{ij}\right) \quad [8]$$

One of the resulting clusters was retained as optimal, indicating the presence of the clay lens.

The second method is based on a map of the probability of the clay lens occurring. This probability map was obtained through IK; the centroid of the optimal cluster from the fuzzy-*k*-means classification was taken as the critical threshold z_c. The resulting probability map was classified into a Boolean map showing predicted absence or presence of the clay lens.

Accuracy Measurements

The results of the delineation methods were compared with a validation image showing the experimentally observed presence of the clay lens. Categorical comparisons are generally based on a confusion matrix containing categorical similarities obtained from a pixel-by-pixel comparison. Table 1 shows a two by two confusion matrix in which the elements are the number of grid cells that fall into each categorical combination. Diagonal elements represent an agreement between the reference and the prediction, and off-diagonal elements represent misclassifications (Congalton and Green, 1999).

A first measure is the overall accuracy (A_o), defined as the number of correctly classified pixels divided by the total number of pixels [$(a + d)/N$]. The main objections to this statistic are (i) its dependence on the prevalence [the frequency of presences $(a + c)/N$; Fielding and Bell, 1997] and (ii) the possibility that a large number of cells can be classified correctly due to chance.

The kappa statistic (κ; Cohen, 1960) eliminates classification agreement by chance. It indicates proportionally how much better the results (proportion observed agreement, P_o) are compared with a purely random classification (proportion expected agreement, P_c); the larger κ, the more accurate the classification. Variants of the standard κ were developed to: (i) correct κ with random chance agreement (κ*) (Foody, 1992); and (ii) quantify how much of the error is due to categorical differences (κ-histo) and locational errors (κ-loc) (Pontius, 2000). Table 2 gives the formulae for the calculation of κ and its variants for a two by two contingency matrix. Foody (1992) showed that the standard κ overestimates the agreement by chance, and corrected κ to κ* by giving each category an equal membership probability (0.5 in case of two categories). The κ* has also been described in the literature as an adjustment to κ for a prevalence effect, since a skewed distribution of categories increases P_c (Byrt et al., 1993). The standard κ confounds quantification error with location error and Pontius (2000) defined κ as the product of κ-histo and κ-loc. The κ-histo is a measure for the quantitative similarity of two maps, while κ-loc indicates the extent to which the similarity is a result of the spatial distribution of cells. For delineation studies, κ-loc was considered to be more relevant than κ-histo.

Table 2. Formulae to calculate the kappa statistic (κ) and its variants from a two by two confusion matrix.

κ and variants†	Formula‡
κ	$\frac{P_o - P_c}{1 - P_c}$ with $P_o = \frac{a+d}{N}$ and $P_c = \frac{(a+c)(a+b)+(b+d)(c+d)}{N^2}$
κ*	$\frac{P_o - 0.5}{1 - 0.5}$
κ-histo	$\frac{P_{max} - P_c}{1 - P_c}$ with $P_{max} = \frac{\mathrm{Min}(a+b, a+c) + \mathrm{Min}(c+d, b+d)}{N}$
κ-loc	$\frac{P_o - P_c}{P_{max} - P_c}$

† κ*, κ corrected with random agreement; κ-histo, the proportion of error due to categorical differences; κ-loc, the proportion of error due to categorical differences.

‡ P_o, proportion of observed agreement; P_c, proportion of expected agreement.

A disadvantage of pixel-based measures is that a similarity of spatial patterns is not captured. The Map Comparison Kit (MCK) software provides methods for pattern recognition (Visser and de Nijs, 2006). Hagen (2003) proposed a fuzzy set approach to calculate κ, taking into account the fuzziness of category and location. The degree of uncertainty or "vagueness" among categories is set with the fuzzy category matrix. The fuzziness of location is set with a function (exponential, linear, or constant decay) that defines the level to which the neighboring cells influence the target cell. The fuzzy set map comparison results in a fuzzy similarity map from which the average similarity (S_a) is calculated, representing an overall quantitative measure of similarity. Values of S_a vary between 1 for identical maps and 0 for fully distinct maps. For a full theoretical description, see Hagen-Zanker et al. (2005).

To validate the probability map a receiver operating characteristic (ROC) curve can be constructed (Pontius and Schneider, 2001). The ROC curve relates relative proportions of correctly classified cells [$a/(a + c)$] and incorrectly classified cells [$b/(b + d)$] across a continuous range of probability thresholds. The area under this curve (AUC) is a measure of the ability to correctly discriminate between the absence and the presence of an event of interest—in our case, the clay lens. An AUC of 0.5 (a diagonal line on the curve) indicates a classification performance no better than chance, while a classification with perfect discrimination has an AUC of 1. Manel et al. (2001) showed that the AUC statistic is prevalence independent.

Besides for accuracy purposes, information from the contingency matrix was also used to determine the optimal probability threshold through the F measure. The F measure is defined as the harmonic mean of precision (P) and recall (R) where precision is the proportion of presences that are real presences [$P = a/(a + b)$] and recall is the proportion of correctly classified presences [$R = a/(a + c)$]. A weighted version of the F measure (van Rijsbergen, 1979) was used:

$$F_\beta = \frac{(\beta^2 + 1)PR}{\beta^2 P + R} \quad [9]$$

with $\beta \in [0,+\infty]$ as a weighting factor controlling the relative importance of precision vs. recall. With $\beta = 1$, precision and recall have equal weights; a smaller β emphasizes precision, a larger β emphasizes recall. In this study, β was set to 0.5 and $F_{0.5}$ was maximized to select the optimal probability threshold.

RESULTS AND DISCUSSION

Apparent Electrical Conductivity Measurements

The locations of the 156 ECa measurements are shown in Fig. 1a. The descriptive statistics of the EM38DD measurements (Table 3) show that the ECa values of this sandy soil were very low (3–9 mS m^{-1}) with relatively small CVs (22 and 29% for EC_h and EC_v, respectively). The EC_h and EC_v measurements had similar mean values within the same data range. Their distribution was symmetrical but platykurtic, whereas the PR measurements showed a skewed, leptokurtic distribution. In most studies, the correlation between EC_h and EC_v has been reported to be very strong (e.g., Triantafilis and Lesch, 2005; Vitharana et al., 2006), but in this study the correlation coefficient was only 0.74, indicating some deviation from a linear relationship.

Spherical variogram models with a nugget effect (C_0) were found to represent the experimental variograms best; these models are defined as follows:

Table 3. Descriptive statistics of electromagnetic induction measurements of electrical conductivity in the horizontal (EC_h) and vertical (EC_v) orientations and the profile ratio (PR) with geostatistical parameters.

Parameter	Summary statistics						Variogram parameters	
	Mean	Min.	Max.	CV†	Skewness	Kurtosis	RNE‡	Range
	mS m^{-1}			%			%	m
EC_h	5.90	3	9	22	0.075	–0.776	10	83
EC_v	6.06	3	9	29	0.206	–1.287	6	78
PR	1.01	0.60	1.75	21	0.933	1.378	30	81.7

† CV, coefficient of variation.

‡RNE, relative nugget effect ($[C_0/(C_0 + C_1)]100$)

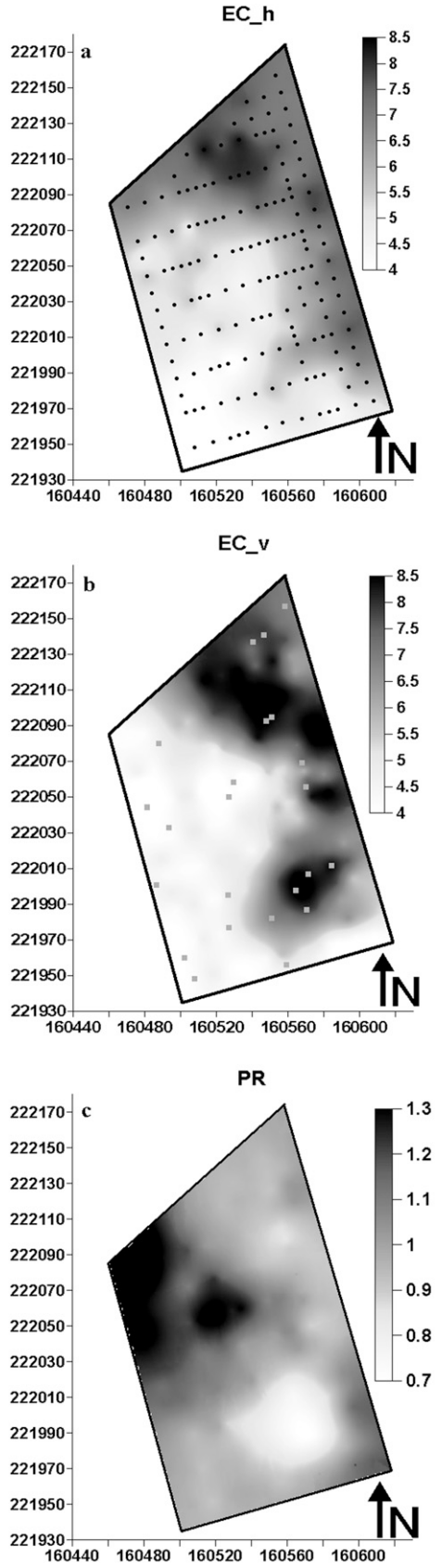

Fig. 1. Point ordinary kriging maps of electrical conductivity (a) using the horizontal orientation (EC_h, mS m^{-1}) with measurement locations of EM38DD (dots) and (b) using the vertical orientation (EC_v, mS m^{-1}) with locations of texture samples (squares), and (c) the profile ratio (PR). (Metric Lambert coordinates on *x* and *y* axes.)

$$\gamma(\mathbf{h}) = \begin{cases} C_0 + C_1\left[1.5\dfrac{\mathbf{h}}{a} - 0.5\left(\dfrac{\mathbf{h}}{a}\right)^3\right], & \text{if } 0 < \mathbf{h} \le a \\ C_0 + C_1, & \text{if } \mathbf{h} > a \end{cases} \quad [10]$$

where $\gamma(\mathbf{h})$ is the semivariance at lag distances **h,** C_1 is the sill, and *a* the range. The variograms of EC_h and EC_v had a similar spatial structure with a strong spatial relation (low relative nugget effect, RNE, of 10 and 6%, respectively), whereas the PR measurements had a larger RNE (30%; Table 3). The RNE measures the proportion of random or short-distance variability (RNE = $[C_0/(C_0 + C_1)]100$). The range of the variograms was on the order of 80 m for all three variables. Although the data range was rather small, maps of EC_h and EC_h, obtained by point OK with a pixel resolution of 1 by 1 m showed clear and rather similar patterns (Fig. 1a and 1b). The highest ECa values occurred in the east of the field, the lowest in the west. The PR map is given in Fig. 1c. It indicates that most of the study site is characterized by a rather homogeneous soil (PR values around 1), but in the northwest corner increased PR values were found (1.2–1.3) whereas in the southeast a circular phenomenon with decreased PR values (0.7–0.8) can be seen.

Clay Content and Apparent Electrical Conductivity Variability

Based on the clay content of the 23 sampled locations (Fig. 1b), two types of textural profiles could be distinguished: one homogeneous with low clay content down to 2 m (18 locations), the other one with a marked increase in clay content from a depth varying between 1 and 2 m downward (five locations) (Fig. 2). The standard deviation of the clay content of the homogeneous soil profile was quite uniform for all layers, on average 2.6%. The top 1 m of the heterogeneous soil profile had a similar standard deviation, but it increased strongly below 1 m to 6.5% on average. This increase in standard deviation resulted from the variable depth at which the clay lens occurred. The heterogeneous soil profiles were all characterized by an increased EC_v, resulting in a decreased PR. The average PR of the heterogeneous profiles was 0.81, compared with an average PR value of 1.03 for the homogeneous soil profiles.

Figure 1c shows that in the northwest corner, the EC_h appeared to be higher than the EC_v, although no substantial textural differences were found in the samples of that area. We assumed that the decrease in EC_h at those places was caused by anthropogenic disturbances influencing the electromagnetic signal. In the southeast, the decreased PR was clearly caused by a textural discontinuity. All samples located in this circular pattern of small PR values had a substantial increase in clay content (between 13 and 27%) at a depth between 1.5 and 2 m.

Table 4 shows the Pearson correlation coefficients (*r*) between the mean clay content in the different soil layers (0.5-m intervals) and EC_h and EC_v. Up to 1.5-m depth, the correlations for both EC_h and EC_v were rather weak ($r <$ 0.50) because of the textural homogeneity. In the 1.5- to 2-m layer, the correlation increased. In particular, EC_v was well related with the more variable clay content in that layer (r = 0.67); with EC_h, the correlation was considerably less (r = 0.41). Looking at the correlation across the whole soil profile, averaged for the top 1.5 and 2 m, the clay content in the 1.5-

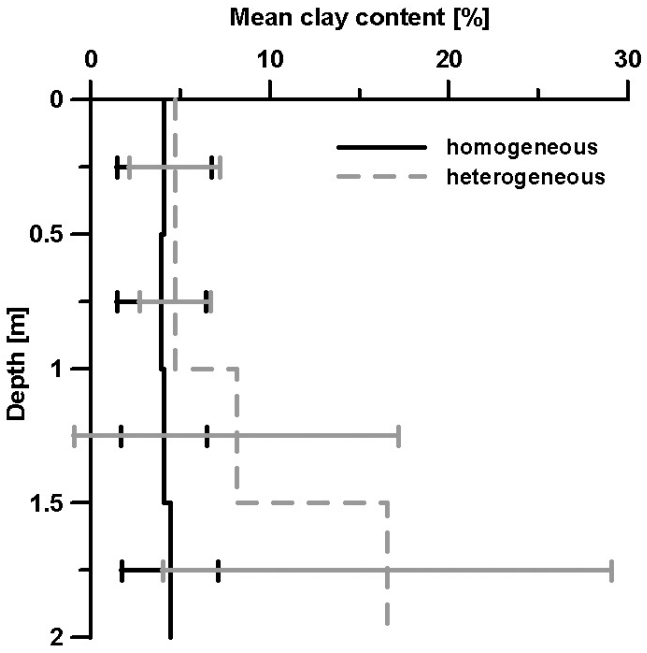

Fig. 2. Mean clay content of the heterogeneous and homogeneous soil profiles, shown in layers of 0.5 m (error bars represent the standard deviation).

to 2-m layer seemed to increase the correlation, especially for EC_v (r increased from 0.44 to 0.56).

Delineation of the Clay Lens

The presence of a clay lens in our sandy soil caused a clear textural heterogeneity, resulting in an increased EC_v compared with EC_h. Therefore PR minima were hypothesized to indicate the presence of this clay lens.

A fuzzy-k-means classification of the interpolated PR values was performed with a fuzzy exponent (φ) of 1.3, which is in the middle of the range 1.12 to 1.5 as suggested for soil data by Odeh et al. (1990). Minimizing the NCE and the FPI resulted in the least fuzzy and least disorganized number of classes (Fig. 3a). The study site was optimally classified into five classes: two classes with a PR centroid around one, two classes with a PR centroid larger than one, and one class with a PR centroid smaller than one (Fig. 3b).

Our interest was with the class with the lowest PR centroid (0.81), indicating an increasing conductivity with depth, suggesting the presence of a clay lens. In a first, simple approach, a Boolean image was used to predict the presence of the clay lens (Fig. 4a): centroid PR 0.81 = clay lens, centroid PR > 0.81 ≠ clay lens. This Boolean image resulted in two circular areas, of which the small one seemed to represent no clay lens because in this area both EC_h and EC_v had increased mean values, indicating a larger clay content in the entire profile, but with a slight increase with depth.

The second method used this centroid value of 0.81 as the threshold value z_c in IK. This method introduced uncertainty in terms of the probability that a clay lens is present. Based on the global ccdf of the PR observations, seven thresholds (z_k) were

Table 4. Pearson correlation coefficients for mean clay content (from 23 locations) of different soil layers and apparent electrical conductivity in the horizontal (EC_h) and vertical (EC_v) orientations.

Depth of mean clay content	Pearson correlation coefficient	
	EC_h	EC_v
m		
0–0.5	0.32	0.30
0.5–1	0.37	0.28
1–1.5	0.34	0.38
1.5–2	0.41	0.67**
0–1.5	0.44*	0.44*
0–2	0.40	0.56*

* Significant at the 0.05 level.

** Significant at the 0.01 level.

selected for the indicator coding of PR. These thresholds correspond to the deciles of the PR distribution, since the 0.4, 0.5, 0.6, and 0.7 deciles had the same quantile with a value of 1. Because a small PR indicates a textural heterogeneity, the clay lens was assumed to occur at locations with a PR ≤ 0.81. Indicator kriging provided the probability that PR ≤ 0.81, which was taken as a measure of prediction that a clay lens occurs (Fig. 4b).

Validation

All auger observations (those performed for the textural analyses and the binary observations used for the validation) were binary coded: 1 if a clay lens occurred within a depth of 2 m, 0 if it did not occur. These values were interpolated using IK with a spherical variogram model having a RNE of 11% and a range of 90 m (Fig. 5a), resulting in an indicator map of the presence of a clay lens. This map was categorized by a threshold of 0.5: whenever the estimated indicator was at least 0.5, a clay lens was expected. This map was taken as the validation image (Fig. 5b). Figure 5b also shows the sampled locations as white dots when the clay lens was observed within 2 m, or as black dots if no clay lens was encountered.

Using this validation image, the accuracy of the delineation methods was evaluated. First, the probability map of the second method was classified into a Boolean image based on an optimal

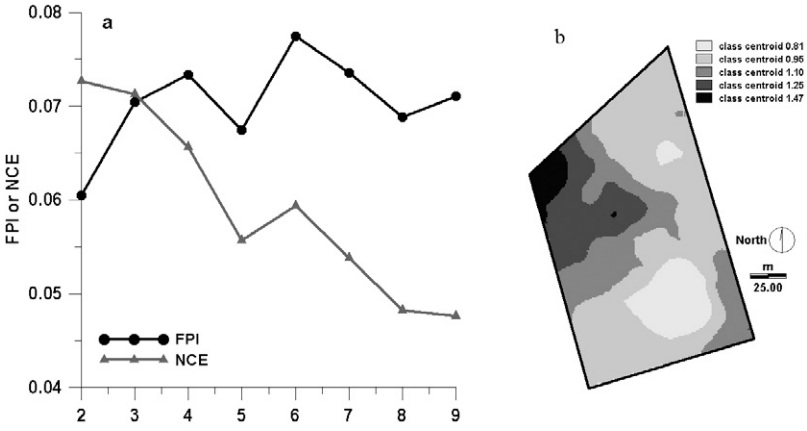

Fig. 3. (a) Fuzziness performance index (FPI) and normalized classification entropy (NCE) as a function of the number of classes, and (b) map of fuzzy classification of the profile ratio into five classes.

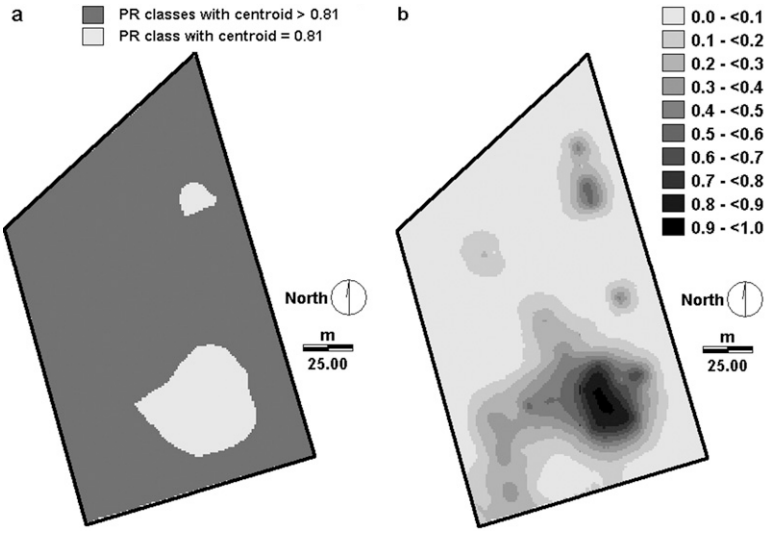

Fig. 4. Prediction of the clay lens according to (a) the fuzzy-*k*-means reclassification and (b) the indicator kriging probability map showing the probability that the profile ratio is ≤ 0.81.

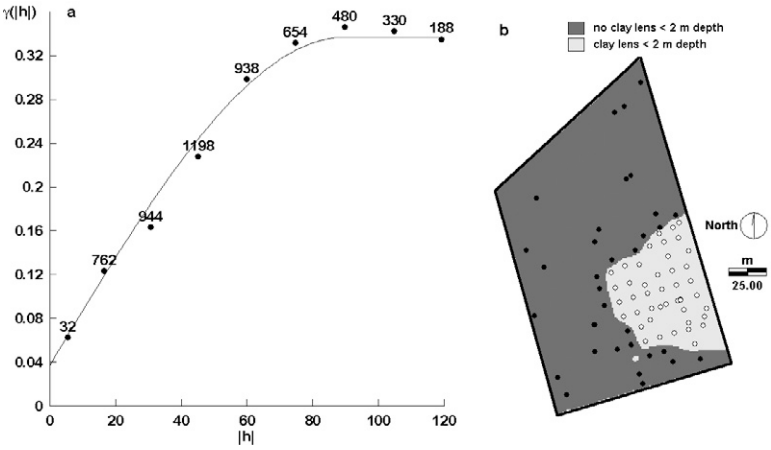

Fig. 5. (a) Indicator variogram model of the validation data (dots with number of data pairs) and (b) the validation image.

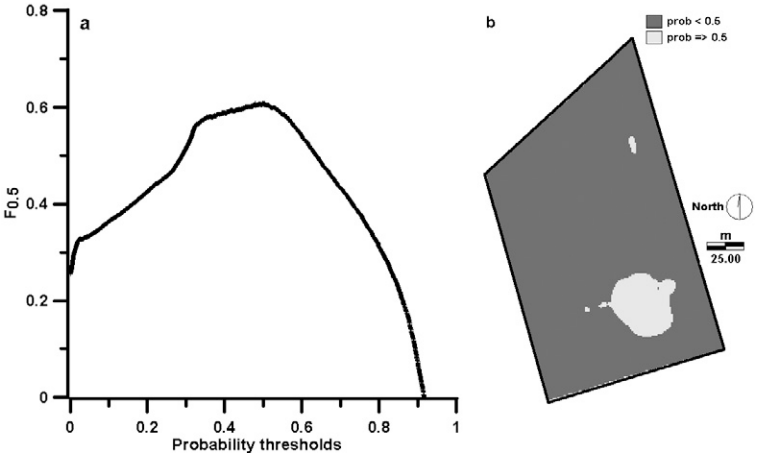

Fig. 6. (a) The measure of the harmonic mean of precision and recall weighted at 0.5 ($F_{0.5}$) in function of probability thresholds and (b) classification of the indicator kriging probability map (with a probability threshold of 0.50).

probability value determined with the $F_{0.5}$ measure. The $F_{0.5}$ measure was maximized at a probability value of 0.50 (Fig. 6a). All pixels with a probability ≥ 0.50 were classified into a class where the clay lens was predicted to occur (Fig. 6b).

The similarity between the presence/absence pattern of the two Boolean classifications and the validation image can be seen clearly (Fig. 4a, 5b, and 6b). Nevertheless, there was a substantial difference in terms of the size of the clay lens: the area of the clay lens was 0.25 and 0.14 ha for the two Boolean classifications, whereas the validation image showed a clay lens of 0.47 ha. So the location of the clay lens was correct, but the spatial extent of the clay lens was underestimated by both methods. The main error occurred at the eastern boundary of the clay lens. This side is near a metal fence that delimits the study site. This might have influenced the electromagnetic field induced by the EM38DD and the resulting ECa measurements.

To quantify the accuracy of the two methods, the Boolean maps were compared with the validation image on a pixel-by-pixel basis. Table 5 shows the resulting accuracy measures. The A_o reached high values for both methods (0.819–0.838), but it should be noted that there was a prevalence effect of 21%; the proportion of pixels without an increase in subsoil (<2 m) clay is larger than with presence of the clay lens. Predicting the absence of the clay lens in the whole study site would still give an A_o of 0.79. The κ values were 0.341 and 0.349 for the two methods, respectively, indicating a fair agreement (Landis and Koch, 1977). After correction for the prevalence effect, a substantial strength of agreement was reached, indicated by κ* values of 0.634 and 0.676. In terms of κ-loc, the IK method scored best with a κ-loc of 0.86. The spatial context was taken into account with S_a. Fuzziness of category was not considered and fuzziness of location was set with an exponential decay function (with a halving distance of two cells and a neighborhood defined by a radius of two cells). This measure was, for both methods, higher (0.819 and 0.841) than the indices calculated on a pixel basis. So we can conclude that the delineation was good in terms of spatial agreement. The IK-based method was found to be the most accurate, but it is also a more elaborate method based on a PR threshold value obtained from the fuzzy-*k*-means method. Nevertheless, the IK-based method was preferred to delineate the clay lens.

The accuracy of the probability method was also confirmed by the ROC curve. The AUC value of this curve was 0.770 with a standard deviation of 0.004, indicating that in 77% of all instances, the method allowed correct discrimination between the presence and absence of the clay lens. Following Swets (1988), an AUC value between 0.7 and 0.9 indicates reasonable discriminating ability. Thus processing the EM38DD measurements allows delineation of a clay lens in a sandy soil with an acceptable level of accuracy.

Depth of the Clay Lens

The depth to the upper boundary of a clay layer (D_c) was reported to be an important factor for biomass development in pine stands (Usoltsev and Vanclay, 1995). In our study site, a significant relationship between D_c (measured at 42 locations) and EC_v was found, with a Pearson cor-

Table 5. Accuracy measures of the two classification methods.

Accuracy measure†	Fuzzy-*k*-means	Classification of indicator kriging probability map
A_o	0.817	0.838
κ	0.341	0.349
κ*	0.634	0.676
κ-loc	0.529	0.864
S_a	0.819	0.841

† A_o, overall accuracy; κ*, κ corrected with random chance agreement; κ-loc, proportion of error due to locational errors; S_a, average similarity.

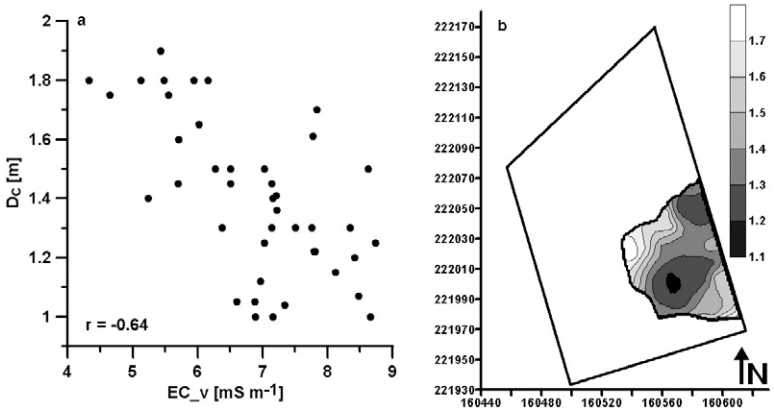

Fig. 7. (a) Scatterplot of electrical conductivity in the vertical orientation (EC_v) vs. the depth of the clay lens (D_c), and (b) the depth of the textural discontinuity (clay lens in meters below the surface and metric Lambert coordinates on *x* and *y* axes).

relation coefficient of −0.64 (Fig. 7a). The closer the textural discontinuity was to the surface, the more it contributed to the response of the sensor. Following Doolittle et al. (1994), we fitted an exponential regression model, which appeared to be the best model to predict D_c (Fig. 7b):

$$D_c = 0.986 + \exp(1.438 - 0.347\ \text{EC\_v}) \quad (R^2 = 0.43) \qquad [11]$$

The central part of the clay lens occurred closest to the surface, with a minimum depth of 1.1 m.

CONCLUSIONS

Analyzing the EM38DD data resulted in an accurate identification of the location of the clay lens, but tended to underestimate its spatial extent. Indicator kriging appeared to be the most appropriate processing technique through the use of a probability map showing the probability of the clay lens to occur. The fuzzy-*k*-means algorithm was used as an initial step to determine the optimal (and objective) PR threshold. In delineation studies, the spatial context of similarities should be taken into account; both κ-loc and S_a were found to give good results.

This sensor appeared to be a suitable instrument for detecting lateral and vertical soil textural variability important for forest management applications. To determine a pedological discontinuity, both orientations of the EM38DD sensor were essential because only the PR value was useful for analyzing the vertical heterogeneity of the soil profile. We concluded that the dual dipole version of the sensor allows extra opportunities for EMI applications. One field survey with the EM38DD is sufficient to characterize the spatial textural variability, to locate the presence of a clay lens, and to map its depth approximately.

REFERENCES

Bezdek, J.C. 1981. Pattern recognition with fuzzy objective function algorithms. Plenum Press, New York.

Boll, J., R.P.G. van Rijn, K.W. Weiler, J.A. Ewen, J. Daliparthy, S.J. Herbert, and T.S. Steenhuis. 1996. Using ground-penetrating radar to detect layers in a sandy field soil. Geoderma 70:117–132.

Bork, E.W., N.E. West, J.A. Doolittle, and J.L. Boettinger. 1998. Soil depth assessment of sagebrush grazing treatments using electromagnetic induction. J. Range Manage. 51:469–474.

Bravo, F., and G. Montero. 2001. Site index estimation in Scots pine (*Pinus sylvestris* L.) stands in the High Ebro Basin (northern Spain) using soil attributes. Forestry 74:395–406.

Brus, D.J., M. Knotters, W.A. van Dooremolen, P. van Kernebeek, and R.J.M. van Seeters. 1992. The use of electromagnetic measurements of apparent soil electrical conductivity to predict the boulder clay depth. Geoderma 55:79–93.

Butnor, J.R., J.A. Doolittle, K.H. Johnson, L. Samuelson, T. Stokes, and L. Kress. 2003. Utility of ground-penetrating radar as a root biomass survey tool in forest systems. Soil Sci. Soc. Am. J. 67:1607–1615.

Byrt, T., J. Bishop, and J.B. Carlin. 1993. Bias, prevalence, and kappa. J. Clin. Epidemiol. 46:423–429.

Cohen, J. 1960. A coefficient of agreement for nominal scales. Educ. Psychol. Meas. 20:37–46.

Congalton, R., and K. Green. 1999. Assessing the accuracy of remotely sensed data: Principles and practices. Lewis Publ., New York.

Corwin, D.L., S.R. Kaffka, J.W. Hopmans, Y. Mori, J.W. van Groenigen, C. van Kessel, S.M. Lesch, and J.D. Oster. 2003. Assessment and field-scale mapping of soil quality properties of a saline sodic soil. Geoderma 114:231–259.

Corwin, D.L., and S.M. Lesch. 2005. Apparent soil electrical conductivity measurements in agriculture. Comput. Electron. Agric. 46:11–43.

Deutsch, C.V., and A.G. Journel. 1998. GSLIB: Geostatistical software library and user's guide. 2nd ed. Appl. Geostat. Ser. Oxford Univ. Press, Oxford, UK.

Doolittle, J.A., and M.E. Collins. 1998. A comparison of EM induction and GPR methods in areas of karst. Geoderma 85:83–102.

Doolittle, J.A., K.A. Sudduth, N.R. Kitchen, and S.J. Indorante. 1994. Estimating depths to claypans using electromagnetic induction methods. J. Soil Water Conserv. 49:572–575.

Fielding, A.H., and J.F. Bell. 1997. A review of methods for the assessment of prediction errors in conservation presence/absence models. Environ. Conserv. 24:38–49.

Foody, G.M. 1992. On the compensation for chance agreement in image classification accuracy assessment. Photogramm. Eng. Remote Sens. 58:1459–1460.

Gish, T.J., W.P. Dulaney, K.-J.S. Kung, S.C.T. Daughtry, J.A. Doolittle, and P.T. Miller. 2002. Evaluating use of ground-penetrating radar for identifying subsurface flow pathways. Soil Sci. Soc. Am. J. 66:1620–1629.

Gomez, A., R.F. Powers, M.J. Singer, and W.R. Horwath. 2002. Soil compaction effects on growth of young ponderosa pine following litter removal in California's Sierra Nevada. Soil Sci. Soc. Am. J. 66:1334–1343.

Goovaerts, P. 1997. Geostatistics for natural resources evaluation. Oxford Univ. Press, Oxford, UK.

Hagen, A. 2003. Fuzzy set approach to assessing similarity of categorical maps. Int. J. Geogr. Inf. Sci. 17:235–249.

Hagen-Zanker, A., B. Straatman, and I. Uljee. 2005. Further development of a fuzzy set map comparison approach. Int. J. Geogr. Inf. Sci. 19:769–785.

Inman, D.J., R.S. Freeland, J.T. Ammons, and R.E. Yoder. 2002. Soil investigations using electromagnetic induction and ground-penetrating radar in southwest Tennessee. Soil Sci. Soc. Am. J. 66:206–211.

Kung, K.-J.S., and S.V. Donohue. 1991. Improved solute-sampling protocol in a sandy vadose zone using ground-penetrating radar. Soil Sci. Soc. Am. J. 55:1543–1545.

Landis, J.R., and G.G. Koch. 1977. The measurement of observer agreement for categorical data. Biometrics 33:159–174.
Lark, R.M., and R.B. Ferguson. 2004. Mapping risk of soil nutrient deficiency or excess by disjunctive and indicator kriging. Geoderma 118:39–53.
Manel, S., H.C. Williams, and S.J. Ormerod. 2001. Evaluating presence–absence models in ecology: The need to account for prevalence. J. Appl. Ecol. 38:921–931.
McBride, R.A., A.M. Gordon, and S.C. Shrive. 1990. Estimating forest soil quality from terrain measurements of apparent electrical conductivity. Soil Sci. Soc. Am. J. 54:290–293.
McNeill, J.D. 1980. Electromagnetic terrain conductivity measurement at low induction numbers. Tech. Note TN-6. Geonics Ltd., Mississauga, ON, Canada.
Mueller, T.G., N.J. Hartsock, T.S. Stombaugh, S.A. Shearer, P.L. Cornelius, and R.I. Barnhisel. 2003. Soil electrical conductivity map variability in limestone soils overlain by loess. Agron. J. 95:469–507.
Odeh, I.A.O., A.B. McBratney, and D.J. Chittleborough. 1990. Design of optimal sampling spacings for mapping soil using fuzzy-*k*-means and regionalized variable theory. Geoderma 47:93–122.
Ogg, C.M., W.J. Edmonds, and J.C. Baker. 2000. Statistical verification of soil discontinuities in Virginia. Soil Sci. 165:170–183.
Pontius, R.G., Jr. 2000. Quantification error versus location error in comparison of categorical maps. Photogramm. Eng. Remote Sens. 66:1011–1013.
Pontius, R.G., Jr., and L.C. Schneider. 2001. Land-cover change model validation by an ROC method for the Ipswich watershed, Massachusetts, USA. Agric. Ecosyst. Environ. 85:239–248.
Roubens, M. 1982. Fuzzy clustering algorithms and their cluster validity. Eur. J. Oper. Res. 10:294–301.
Samouëlian, A., I. Cousin, A. Tabbagh, A. Bruand, and G. Richard. 2005. Electrical resistivity survey in soil science: A review. Soil Tillage Res. 83:173–193.
Schoenholtz, S.H., H. Van Miegroet, and J.A. Burger. 2000. A review of chemical and physical properties as indicators of forest soil quality: Challenges and properties. For. Ecol. Manage. 138:335–356.
Soil Survey Staff. 2003. Keys to Soil Taxonomy. 9th ed. NRCS, Washington, DC.
Swets, J.A. 1988. Measuring the accuracy of diagnostic systems. Science 240:1285–1293.
Triantafilis, J., and S.M. Lesch. 2005. Mapping clay content using electromagnetic induction techniques. Comput. Electron. Agric. 46:203–237.
Usoltsev, V.A., and J.K. Vanclay. 1995. Stand biomass dynamics of pine plantations and natural forests on dry steppe in Kazakhstan. Scand. J. For. Res. 10:305–312.
Van Meirvenne, M., and P. Goovaerts. 2001. Evaluating the probability of exceeding a site-specific soil cadmium contamination threshold. Geoderma 102:75–100.
van Rijsbergen, C.J. 1979. Information retrieval. Butterworths, London.
Visser, H., and T. de Nijs. 2006. The map comparison kit. Environ. Modell. Softw. 21:346–358.
Vitharana, U.W.A., M. Van Meirvenne, L. Cockx, and J. Bourgeois. 2006. Identifying potential management zones in a layered soil using several sources of ancillary information. Soil Use Manage. 22:405–413.
Woolery, M., K. Olson, J. Dawson, and G. Bolero. 2002. Using soil properties to predict forest productivity in southern Illinois. J. Soil Water Conserv. 57:37–45.